Nonlinearity Engineering with the Quarton

by

Yufeng Ye

B.ASc., University of Toronto (2019)

Submitted to the Department of Electrical Engineering and Computer Science
in partial fulfillment of the requirements for the degree of

Master of Science in Electrical Engineering and Computer Science

at the

MASSACHUSETTS INSTITUTE OF TECHNOLOGY

May 2020

Author .....
Department of Electrical Engineering and Computer Science
May 15, 2020

Certified by .....
Kevin P. O'Brien
Assistant Professor of Electrical Engineering and Computer Science
Thesis Supervisor

Accepted by .....
Leslie A. Kolodziejski
Professor of Electrical Engineering and Computer Science
Chair, Department Committee on Graduate Students

Nonlinearity Engineering with the Quarton

by

Yufeng Ye

Submitted to the Department of Electrical Engineering and Computer Science
on May 15, 2020, in partial fulfillment of the
requirements for the degree of
Master of Science in Electrical Engineering and Computer Science

Abstract

In this thesis, we show the principles and applications of a new technique we call "nonlinearity engineering" using a recent superconducting qubit, the Quarton. In traditional nonlinear optics, nonlinear effects are usually weak perturbations to linear interactions. Similarly, microwave quantum optics with superconducting circuits relies on the Josephson junction for a negative Kerr nonlinearity that is much weaker than its associated linear energy. Recently, a new superconducting qubit known as the "Quarton" can offer non-perturbatively strong nonlinearity. Here, we demonstrate the general principle of using the Quarton's positive Kerr and zero linear energy to perform nonlinearity engineering, i.e. the selective design of the nonlinear properties of microwave artifical atoms, metamaterials, and photons in a manner that (to the best of our knowledge) has no optical analog. We show that for Quarton mediated light-matter coupling, the Quarton can erase or amplify the nonlinearity of artificial atoms and metamaterials. Without nonlinearity, matter behaves light-like and we find (to our best knowledge) the first theoretical demonstration of cross-Kerr between linear microwave photon modes. We extend these fundamental results and provide a practical application by designing a Josephson traveling wave photon detector.

Thesis Supervisor: Kevin P. O'Brien
Title: Assistant Professor of Electrical Engineering and Computer Science

Acknowledgments

I have been extremely blessed to have met all the amazing people in my life that made this thesis possible. They are my family and friends, my mentors, my peers, and the many kind strangers along the way. This thesis is dedicated to them.

I'd like to begin by thanking my advisor Kevin O'Brien. Before joining his group, my mental stereotype of a PhD advisor was that of an old-fashioned scholar perpetually out-of-reach to students, communicates in ancient cryptic languages, and performs black arts in the laboratory. I never imagined having an advisor as open-minded, supportive, and genuinely caring as Kevin. I am extremely grateful for his guidance along the way, both academic and personal.

I'd like to thank QCE, Greg, Mahdi, Kaidong, and our collaborators Arne Grimsmo and Will Oliver for their support, helpful insights, and discussions throughout this intellectual journey.

I owe a huge debt of gratitude to my previous advisors Alexandre Blais and Nazir Kherani, and mentors Andrew Flood, Baptiste Royer, and Joel Loh. I am thankful for their guidance during my undergrad.

Finally, none of this would have been possible without the loving support of my family. I'd like to thank my parents for their unconditional support. I'd like to thank Run for her love and companionship.

I'd also like to thank my friends Sophia, Zhen, Yang, Junhong and Guang, Zhuquan, Peter and other friends at the H & M Cooking Group; as well as Ruicong, Yujie, Peiqi, Devany and others from the Avalon game group; and lastly all the amazing people at MIT Singing for Service.

My old friends Raymond and Weiran have been with me every step along the way, and I'm forever grateful for their friendship.

This work is supported by funding from the MIT Center for Quantum Engineering via support from the Laboratory for Physical Sciences and the MIT EECS department in the form of the Jin Au Kong fellowship.

Contents

List of Figures

Chapter 1

Introduction

Superconducting quantum circuits has emerged as one of the most promising hardware platforms for quantum information processing [4, 10]. For its high coherence, ease of fabrication, and vast range of engineering tunability, superconducting qubits and metamaterials have been used extensively for many quantum information applications [16]. In quantum computing, superconduciting qubits have recently enabled the first demonstration of quantum supremacy [2]. In quantum communication and sensing, secure protocols [30] and digital radars [3] have been successfully demonstrated. In addition, the strong light-matter coupling achievable in circuit QED setups (coupling of microwave photons with superconducting qubits) have found new regimes of physics beyond the Jaynes-Cummings model [33], and enabled many hybrid quantum systems [9].

This rising field of circuit QED / microwave quantum optics has its roots in the more traditional disciplines of condensed matter, atomic and molecular optics (AMO), and nonlinear optics.

In this thesis, we find it fruitful to take the more traditional perspectives and use the familiar languages of nonlinear optics and AMO. We will consistently describe superconducting qubits and microwave transmission line waveguides as artificial atoms and metamaterials. We will speak of the nonlinear susceptibility $\chi^{(3)}$, and the "atomic" or "photonic" nature of qubits and waveguides. The analogy between these fields lead to fundamental insights that should hopefully appeal to a broad audience.

1.1 Thesis structure

The thesis will be structured as follows:

In Chapter 2, the background chapter, we introduce some basic background intended for a general audience who may be unfamiliar with superconducting quantum circuits. More advanced background literature will be included, when applicable, at the beginning of other chapters. In this chapter, we show that macroscopic quantum phenomena displayed by superconductivity is at the heart of superconducting circuits. Coherent tunneling of Cooper pairs across a Josephson junction lead to the celebrated Josephson effect. We then introduce the formalism of circuit quantization with the most important example of the quantum LC oscillator. In the next section, we focus on qubits and how they serve as artifical atoms. We show how Josephson junctions serve as nonlinear inductors, and we show the fundamentals of the most common qubit, the transmon. Finally, we introduce metamaterials. We introduce the ABCD matrix formalism and apply it to linear waveguides which can be designed to behave like left-handed, right-handed or both left and right-handed electromagnetic materials.

In Chapter 3, we start our derivation on how the nonlinearities of superconducting circuit elements can be custom designed. We provide deeply insightful derivation for the existence of a superconducting qubit, known as the Quarton [46], which has no linear property and solely nonlinear property. The importance of the Quarton as a maximally nonlinear element follows naturally from our derivation.

In Chapter 4, we focus on exploiting the properties of the purely nonlinear Quarton to create novel light-matter couplings between resonators and qubits. We consider a simple circuit with two qubits coupled by a Quarton. We show that the Quarton can erase or amplify the nonlinearity of artificial atoms and metamaterials. Without nonlinearity, matter behaves light-like, and therefore we show that we can achieve three broad classes of nonlinear couplings: The longitudinal zz coupling between qubits, the AC-Stark coupling between qubit and resonator, and the cross-Kerr coupling between resonators. To our best knowledge, the latter is the first theoretical

demonstration of nonlinear coupling of linearly uncoupled linear microwave photon modes.

In Chapter 5, last main chapter, we extend the derivations for single modes to multi-mode metamaterials. We then turn to the important application of a Josephson traveling wave photon detector (JTWPD). Making use of nonlinearity engineering, we design an ideal implementation of the JTWPD: two nonlinearly coupled but linearly uncoupled linear waveguides.

We conclude the thesis in Chapter 6 by offering a summary of the significant results.

Chapter 2

Background

2.1 Superconductivity and the Josephson junction

Here, we give a brief introduction to superconductivity and the Josephson effect. We will only cover the bare minimum required to understand operations of superconducting quantum devices, we direct interested readers to classic texts [34] for more a in-depth introduction.

Superconductivity is current flow without resistance, it occurs when two electrons pair up to form a special ground state ("Cooper pair"). Physically, the electrons feel an effective attractive force due to exchange of virtual phonons [14]. These Cooper pairs are stable and require 2Δ of energy to break apart and create an excited state. As a result, the number of effective degrees of freedom can be dramatically reduced and we can model superconducting qubits made up of $10^9 - 10^{12}$ of atoms as essentially a single-electron atom [14]. This behavior is achieved by working at low temperature and low frequency ($k_{\mathrm{B}}T, \hbar\omega \ll 2\Delta$), so we can ignore all the non-superconducting excited states of the system. It is worth remarking that superconductivity has thus enabled a macroscopic system to behave quantum mechanically.

Note that we will be working with metal superconductors at microwave frequencies of order GHz. At this frequency, plasma oscillations of the metals (of order 100 THz) will not be excited. Classically, this means the electrons of the metal superconductor are fast and dense enough to screen out a slowly oscillating microwave external field.

Quantum mechanically, this means that the high frequency plasmon modes of the circuit will not be excited and we can safely ignore these modes with the knowledge that they are always in the ground state. Working in this regime is critical because when this approximation breaks down, we have decays of the plasmon modes into single-particle excitations ("Landau-damping") [14]. For readers familiar with surface plasmon polaritons, this choice of low frequency oscillation regime makes the light-matter interaction between light and the superconducting matter more 'light-like' as the superconductor oscillations are approximately dispersionless and can be modeled as stationary photons [9].

Coherent tunneling in Josephson junctions

In non-superconducting tunnel junctions made up of metal - thin oxide - metal, the quantum level spacings are extremely dense and can thus be modelled as a continuum. Therefore, the quantum-mechanical tunneling of electrons across the thin oxide is an incoherent process well-described by Fermi's Golden Rule.

With superconducting junctions, the superconductivity of the metals lead to a 2Δ separation between the ground state and the densely spaced excited states (approximated as continuum). Therefore, again considering only the ground states, we have now a coherent tunneling process where Cooper pairs are exchanged. Mathematically, the tunneling Hamiltonian H_T couples discrete eignestates (labelled by number of Cooper pairs $|m\rangle$) of the two superconducting electrodes [14]:

$$H_{\mathrm{T}} = -\frac{1}{2}E_{\mathrm{J}}\sum_{m}\{|m\rangle\langle m+1| + |m+1\rangle\langle m|\} \tag{2.1}$$

where E_J is the Josephson coupling energy. For readers familiar with condensed matter, this is a simple one-dimensional lattice model with nearest-neighbor hopping with amplitude E_J. This has eigenfunctions $|\varphi\rangle$ [14]:

$$|\varphi\rangle = \sum_{m=-\infty}^{+\infty} e^{+im\varphi}|m\rangle \tag{2.2}$$

$$H_{\mathrm{T}}|\varphi\rangle = -E_{\mathrm{J}}\cos\varphi|\varphi\rangle \tag{2.3}$$

Therefore, the net current flow given by the $\frac{\partial}{\partial\varphi}$ derivative of energy leads to the DC Josephson relation:

$$I(\varphi) = 2e\frac{1}{\hbar}\frac{\partial}{\partial\varphi}\left[-E_{\mathrm{J}}\cos\varphi\right] = \frac{2e}{\hbar}E_{\mathrm{J}}\sin\varphi \tag{2.4}$$

It will be convenient to define the magnetic flux quantum:

$$\Phi_0 = \frac{h}{2e}, \tag{2.5}$$

and the reduced magnetic flux quantum:

$$\phi_0 = \frac{\hbar}{2e}. \tag{2.6}$$

If there is a voltage drop V across the junction, we have the AC Josephson equation:

$$\varphi(t) = \int \frac{1}{\phi_0}V dt \tag{2.7}$$

As we will show later, the AC Josephson equation implies that the dimensionless phase φ can be interpreted as a normalized magnetic flux.

2.1.1 External flux and gauge choice

If superconducting wires form a loop, the loop can enclose some magnetic flux (Fig. 2-1a). The classical result [34] for sum of phases differences φ_i over the loop is:

$$\sum_i \varphi_i = 2\pi n + \frac{\Phi_{ext}}{\phi_0}, \tag{2.8}$$

where n is an integer and Φ_{ext} is the external magnetic flux penetrating the loop. (We have made the usual assumption that the flux due to inductance of the loop itself is negligible [34].)

Eqn. 2.8 introduces an important source of tunability in superconducting circuits.

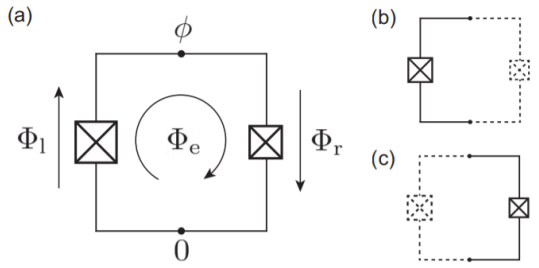

Figure 2-1: a) Superconducting loop threaded by external flux Φ_e (Φ_{ext} in text). Panels b) and c) show two equivalent choices of spanning trees (solid lines) and closure branches (dashed lines) [47].

For a fixed applied Φ_{ext} and n, the constraint introduced by this equation reduces the degrees of freedom of the loop by one. For many important cases such as the SQUID (Superconducting QUantum Interference Device) and flux qubits, the entire circuit element can now be described by a single degree of freedom φ which is tuned by our knob Φ_{ext}. As we will show later, this flux tunability is one necessary ingredient for nonlinearity engineering.

Gauge choice is another important concept necessary to understanding superconducting circuits threaded by external flux. It is well-known that Maxwell's equations have a Gauge symmetry [19]. It can be shown that this gauge freedom allows us to associate a time-independent external flux Φ_{ext} with any potential energy term $U(\varphi)$ of the threaded loop [47]. The branch of $U(\varphi)$ chosen is called "closure branch", and the branch not chosen is known as the "spanning tree" (see Fig. 2-1bc). Essentially, we can choose to shift the potential landscape of any one element in the circuit by flux:

$$U(\varphi) \rightarrow U(\varphi + \frac{\Phi_{ext}}{\phi_0}) \tag{2.9}$$

In practice, the sweet spot flux bias $\Phi_{ext} = \Phi_0/2$ [25] is usually used to shift a JJ potential from cosine to negative cosine:

$$U_{JJ} \propto \cos(\varphi) \rightarrow \cos(\varphi + \pi) = -\cos(\varphi) \tag{2.10}$$

We emphasize here that because *all* choices of spanning tree and closure branch is

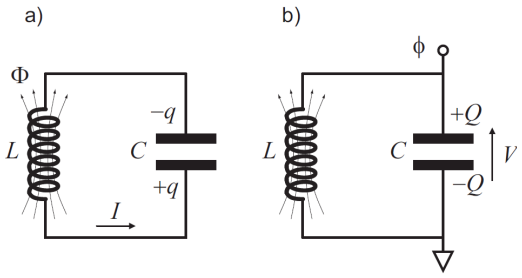

Figure 2-2: Two representations of a LC oscillator. a) In terms of "position" variable charge q and "momentum" variable flux Φ. b) In terms of "position" variable flux ϕ and "momentum" variable charge Q. [14]

equivalent by Gauge freedom, we are free to choose *any* (usually the most convenient) branch and the results we derive will be general. We will invoke this fact when we derive the Quarton.

2.2 Circuit quantization

In this section, we introduce the basic formalism to treat a lumped-element superconducting circuit fully quantum mechanically. The lumped-element regime is valid for circuit components with size much smaller than the microwave wavelengths of light (of order cm). We will focus on the LC oscillator and follow closely the classic derivation [14] to discover that this circuit is exactly analogous to mass-spring systems. The eigenstates are collective oscillations (standing waves) of charge and current in the circuit. We will extend these results to many mode systems including traveling-wave devices in a later section.

Consider a simple LC oscillator as shown in Fig. 2-2a. In terms of capacitor charge q and inductor flux I, we can write the Lagrangian of the circuit as [14]:

$$\mathcal{L} = \frac{1}{2}LI^2 - \frac{1}{2}\frac{q^2}{C} \tag{2.11}$$

Charge conservation implies $I = +\dot{q}$, so we can reduce the Lagrangian to:

$$\mathcal{L} = \frac{L}{2}\dot{q}^2 - \frac{1}{2C}q^2. \tag{2.12}$$

It is worth emphasizing that this is exactly analogous with a mass (L) on a spring (of constant $1/C$), with the charge q serving as position. We can perform the Legendre transform to obtain the Hamiltonian [14]. The "momentum" conjugate to the "position" variable q is the inductor flux Φ:

$$\Phi = \frac{\delta \mathcal{L}}{\delta \dot{q}} = L\dot{q} = LI \tag{2.13}$$

And the Hamiltonian follows:

$$H = \Phi\dot{q} - \mathcal{L} = \frac{\Phi^2}{2L} + \frac{1}{2C}q^2$$

Because we work below the superconducting gap 2Δ, we can quantize the collective circuit modes of q, Φ without regard for the single-particle excitations and high frequency plasmon modes. Introducing the canonical quantization relation between flux $\hat{\Phi}$ and charge $\hat{q}$:

$$[\hat{\Phi}, \hat{q}] = -i\hbar \tag{2.14}$$

We end up obtaining the quantum harmonic oscillator Hamiltonian:

$$H = \frac{\hbar\Omega}{2}\left\{\hat{a}^\dagger\hat{a} + \hat{a}\hat{a}^\dagger\right\} = \hbar\Omega\left\{\hat{a}^\dagger\hat{a} + \frac{1}{2}\right\} \tag{2.15}$$

where $\Omega = \frac{1}{\sqrt{LC}}$ is the natural frequency of the LC oscillator. The energy levels are evenly spaced (Fig. 2-3c). The raising and lowering operators are defined as usual:

$$\hat{a} = +i\frac{1}{\sqrt{2L\hbar\Omega}}\hat{\Phi} + \frac{1}{\sqrt{2C\hbar\Omega}}\hat{q} \tag{2.16}$$

$$\hat{a}^\dagger = -i\frac{1}{\sqrt{2L\hbar\Omega}}\hat{\Phi} + \frac{1}{\sqrt{2C\hbar\Omega}}\hat{q} \tag{2.17}$$

which obey the basic relation

$$\left[\hat{a}, \hat{a}^\dagger\right] = 1 \tag{2.18}$$

We will find that it is easier to integrate the circuit with Josephson junctions (JJ) if we use the flux $\phi(t) = \int^t d\tau V(\tau)$ instead as "position" variable of the LC oscillator

(Fig. 2-2b). This amounts to a trivial rotation of basis, so we will skip the derivation (outlined in [14]).

It will be extremely insightful to write the flux and charge variables in terms of the raising and lowering operators:

$$\begin{aligned} \hat{Q} &= -iQ_{\text{ZPF}}\left(\hat{a} - \hat{a}^\dagger\right) \\ \hat{\phi} &= \Phi_{\text{ZPF}}\left(\hat{a} + \hat{a}^\dagger\right) \end{aligned} \tag{2.19}$$

where we define the extremely important zero point fluctuations:

$$\begin{aligned} Q_{\text{ZPF}} &= \sqrt{\tfrac{C\hbar\Omega}{2}} = \sqrt{\tfrac{\hbar}{2Z}} \\ \Phi_{\text{ZPF}} &= \sqrt{\tfrac{L\hbar\Omega}{2}} = \sqrt{\tfrac{\hbar Z}{2}} \end{aligned} \tag{2.20}$$

where $Z = \sqrt{\frac{L}{C}}$ is the characteristic impedance of the oscillator.

Physically, the size of the zero point fluctuation determines the extent of the wavefunction in that coordinate. Unsurprisingly, this will determine the strength of coupling between two modes as it relates to the degree of overlap of their wavefunction.

2.3 Qubits - artificial atoms

In traditional AMO (atomic and molecular optics) and nonlinear optics, we are limited by nature's atoms. But recall that the electromagnetic response of an atom is usually treated as a driven harmonic oscillator (e.g. Lorentz model). Nonlinearity is incorporated by perturbative inclusion of an anharmonic third order or fourth order potential [5]. So in essence, an atom is just an anharmonic quantum oscillator (for many applications). So if we can engineer an anharmonic quantum oscillator, we should be able to emulate the electromagnetic response of natural atoms. This is, in essence, why superconducting qubits are known as engineered artificial atoms [14, 25].

To have an anharmonic oscillator, we need a source of nonlinearity. The LC oscillator we covered above is completely linear, as it is made of linear inductors and capacitors. To add nonlinearity, we need the Josephson junction (JJ). Recall the

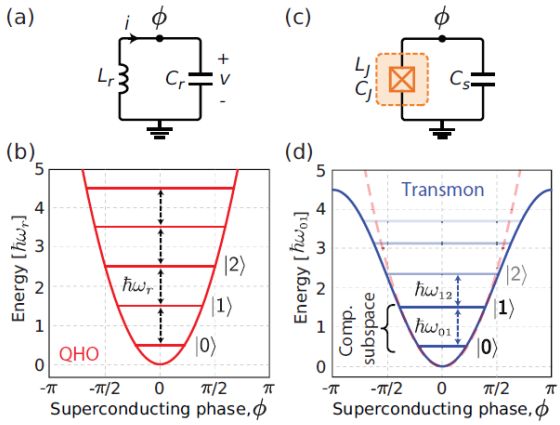

Figure 2-3: Linear resonator vs nonlinear qubit. a) Circuit of linear LC oscillator. b) Energy diagram of the linear resonator. c) Circuit of nonlinear resonator, the cross symbol denotes the JJ. d) Energy diagram of the nonlinear resonator (transmon) that serves as a qubit or artificial atom [25]

potential energy U of the JJ is given by Eqn. 2.3:

$$U = -E_J \cos\varphi \approx E_J(\varphi^2/2 - \varphi^4/24) \tag{2.21}$$

where we Taylor expanded the cosine and left out a constant term that does not contribute to the equations of motion. Because of the AC Josephson equation (Eqn. 2.7), we can draw a direct relation between the superconducting phase variable $\varphi = \int \frac{1}{\phi_0} V dt$ and the magnetic flux $\Phi(t) = \int^t V(\tau) d\tau$ used to define the LC oscillator [14]:

$$\varphi = \frac{\Phi}{\phi_0} \tag{2.22}$$

Recalling that the energy of an inductor L can be written as $\frac{\Phi^2}{2L}$, contrasting this with Eqn. 2.21, we can see the *JJ can be seen as a nonlinear inductor*. We can now define a linear or small-signal JJ inductance L_J:

$$L_J = \frac{\phi_0^2}{E_J}, \tag{2.23}$$

and a general flux tunable nonlinear JJ inductance:

$$L^{-1}(\Phi) \equiv \frac{d^2H}{d\Phi^2} = \frac{1}{L_J}\cos\left(\frac{\Phi}{\phi_0}\right). \tag{2.24}$$

Therefore, if instead of a linear inductor (Fig.2-3a), we used the JJ for the inductance of the LC oscillator (Fig. 2-3c), we obtain the nonlinear anharmonic oscillator we are after. Note that the circuit symbol for the JJ is a cross, as shown in Fig. 2-3c.

We can obtain a perturbative Hamiltonian for this simple qubit formed with a JJ and capacitor. (This family of qubits is known as the Cooper pair box [14], a particular member of this family known as the "transmon" [40] is the most common type of superconducting qubit for its high coherence.) Expanding the φ^4 term in Eqn. 2.21 in terms of $\hat{a}, \hat{a}^\dagger$ defined in Eqn. 2.19, and making the rotating wave approximation (keeping only terms with the same number of $\hat{a}$'s and $\hat{a}^\dagger$'s), we get:

$$H/\hbar = \Omega\hat{a}^\dagger\hat{a} - E_C\hat{a}^{\dagger 2}\hat{a}^2 \tag{2.25}$$

where E_C is the capacitance energy (see [14] for a detailed derivation). Note that this expansion is valid in the limit of small $\varphi_{ZPF} = \Phi_{ZPF}/\phi_0$ or $E_J \gg E_C$. The resulting energy levels are not evenly spaced (Fig. 2-3d).

Note that we can also interpret the Hamiltonian above as that of a Kerr medium with a small Kerr coefficient $K = -E_C$. (Note that here and throughout this thesis, we will adopt the convention which defines the sign of Kerr as the sign of the nonlinar energy term. This may be different from other works in the literature.)

2.4 Waveguides - metamaterials

Metamaterials are engineered artificial material exhibiting exotic physical properties (e.g. negative refraction) that are not found in nature. We will use this term here to describe electromagnetic materials with exotic electric permittivity ϵ and magnetic permeability μ. Metamaterials are classified by their ϵ, μ. A right-handed metamaterial has $\epsilon > 0, \mu > 0$, whereas a left-handed metamaterial has $\epsilon < 0, \mu < 0$.

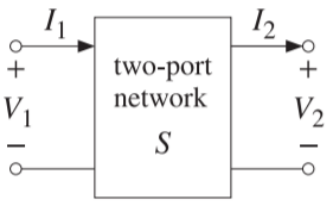

Figure 2-4: Generic two-port network [35]

Because superconducting qubits and circuit QED naturally operate in the microwave regime, we will be reviewing microwave metamaterials [7] based on transmission line waveguides.

In the following section, we will demonstrate the formalism of modeling linear waveguides using the simplest two-port waveguides here, the extension to larger N-port waveguides will follow naturally.

Consider a general two-port network shown in Fig.2-4, it is completely characterized by its input V_1, I_1 and output V_2, I_2 voltage and current response. Common transmission line waveguides can be simply modelled as an infinite periodic sequence of the unit cell two-port network. For any unit cell labelled n, we can capture its input-output response by its ABCD matrix [35]:

$$\begin{bmatrix} V_n \\ I_n \end{bmatrix} = \begin{bmatrix} A & B \\ C & D \end{bmatrix} \begin{bmatrix} V_{n+1} \\ I_{n+1} \end{bmatrix} \tag{2.26}$$

Because we take the transmission line waveguides to be being infinitely long, we can apply the well-known Bloch Theorem. As a result, the unit cell node voltage and currents must only differ by a phase [35]:

$$\begin{aligned} V_{n+1} &= V_n e^{-ika}, \\ I_{n+1} &= I_n e^{-ika}, \end{aligned} \tag{2.27}$$

where a is the unit cell size, and ka is the normalized wavevector.

Combining Eqn. 2.26 and Eqn. 2.27, we find that solving for ka amounts to solving

the eigensystem:

$$\begin{bmatrix} A & B \\ C & D \end{bmatrix} \begin{bmatrix} V_{n+1} \\ I_{n+1} \end{bmatrix} = e^{ika} \begin{bmatrix} V_{n+1} \\ I_{n+1} \end{bmatrix} \tag{2.28}$$

The 2x2 ABCD matrix will admit two eigensolutions corresponding to left and right moving waves.

The characteristic impedance Z_0 is given by the eigenvectors (denoted by superscript e):

$$Z_0 = V^e / I^e \tag{2.29}$$

Because the values of A, B, C, D involve capacitive and inductive circuit impedances, they are in general frequency-dependent. So the eigensolutions and the derived wavevector ka, characteristic impedance Z_0 of the ABCD eigensystem will also be frequency-dependent. We will denote frequency by ω.

To summarize, the procedure for solving a transmission line waveguide system will involve derivation of the unit cell ABCD matrix, solving the eigensystem in Eqn. 2.28, and obtaining the band structure $ka(\omega)$ and impedance $Z_0(\omega)$.

Note that the ABCD matrix formalism applies for both distributed and lumped element unit cells (with different values of A, B, C, D). However, most metamaterials will require engineered circuit components that are commonly realized as lumped elements. So we have made the implicit choice to consider only lumped element unit cells.

Right-, left-, and composite right-/left-handed-handed

Consider the well-known LC ladder in Fig. 2-5a. This is a right-handed material, whereas the inverted structure with series capacitor and ground inductor (Fig. 2-5b) is left-handed [44]. There is a special composite right-/left-handed (CRLH) metamaterial, shown in Fig. 2-5c, that combines with right- and left-handed characteristics.

We can use the ABCD formalism developed above to calculate the behavior of these metamaterials. It is convenient to examine the band structure of the CRLH

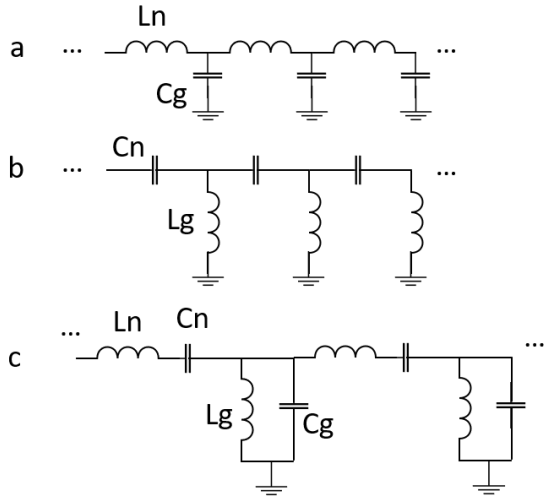

Figure 2-5: a) Right-handed metamaterial. b) Left-handed metamaterial. c) Composite right-/left-handed (CRLH) metamaterial

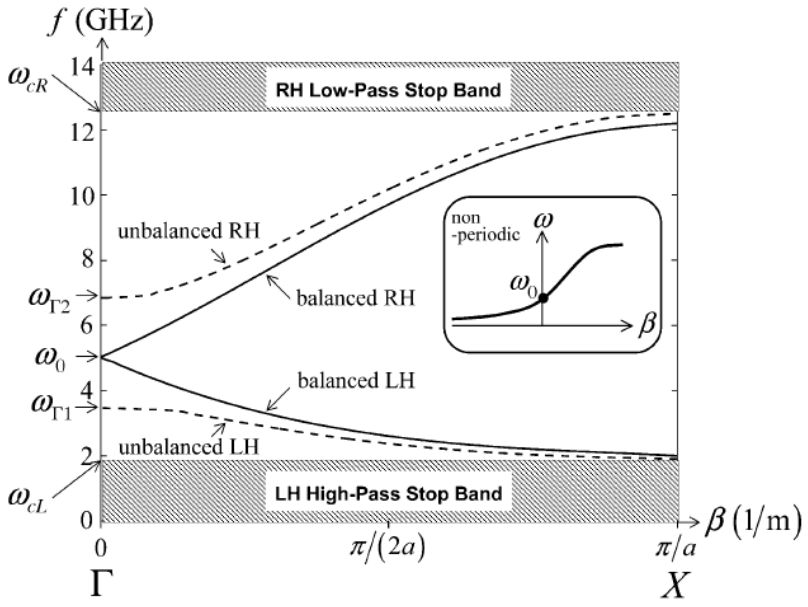

Figure 2-6: Band diagram of CRLH metamaterial showing both left- and right-handed behavior [6].

metamaterial (Fig. 2-6), as it displays both handed behavior. In general, the right-handed medium has a high-frequency cut-off whereas the left-handed medium has a low-frequency cut-off. The CRLH thus has both a high frequency right-handed cut-off ω_{cR} and a low frequency left-handed cutoff ω_{cL} (Fig. 2-6). Unless the CRLH metamaterial is "balanced" [6], there is a bandgap between the left- and right-handed branches of the band diagram.

In general, far away from bandgaps and cut-offs, the waveguide has a characteristic impedance of approximately:

$$Z_0 \approx \sqrt{\frac{L_n}{C_g}} \quad \text{(right-handed)} \tag{2.30}$$

$$Z_0 \approx \sqrt{\frac{L_g}{C_n}} \quad \text{(left-handed)} \tag{2.31}$$

We will discuss the important case of Z_0 near frequency cut-offs in the design for JTWPD in Chapter 5.

Chapter 3

Deriving the Quarton

3.1 Derivation

In traditional nonlinear optics, nonlinear effects are usually weak perturbations to linear interactions. For atoms and materials with centrosymmetric potentials, this can be mathematically described by a weak third order susceptibility $\chi^{(3)} < \chi^{(1)}$ [5]. As we discussed earlier, the JJ also has the centrosymmetric cosine potential, which leads to a weak negative Kerr $|K| \ll \frac{1}{L_J}$. At the qubit level, this weak nonlinearity limits the anharmonicity of qubits and thus their gate speeds. Motivated by faster gates, recently, a new class of qubits [46] were introduced that have a first order quartic potential:

$$U_Q(\phi) \propto E_J\phi^4 + ... \tag{3.1}$$

$$\propto K\phi^4 + ... \tag{3.2}$$

and appropriately named the "Quarton". In this thesis, we use the Quarton not just as a qubit but also as a fundamental nonlinear element that can be viewed as a "plug and play" source of nonlinearity. Because the Quarton has trivial linear properties, it can be used to selectively design the nonlinearity of circuits to remove or add Kerr at will. We will discuss more about this technique we call "nonlinearity engineering" hereafter.

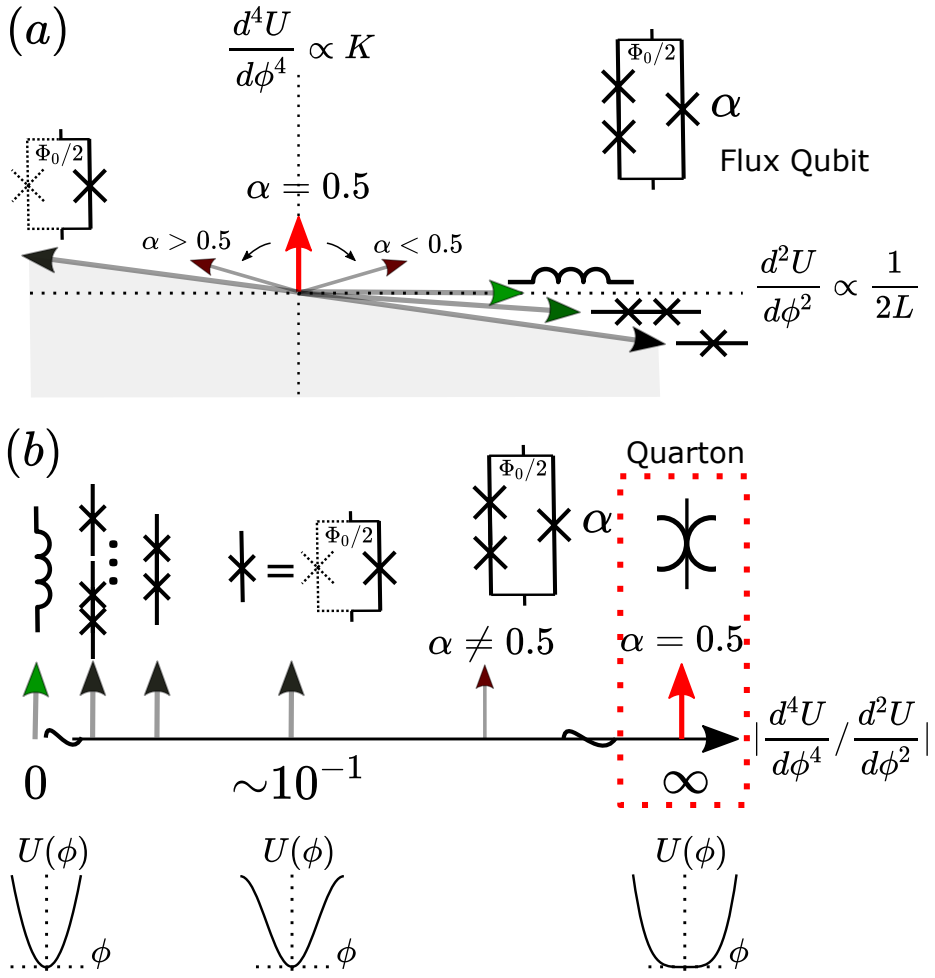

Figure 3-1: Quarton as a purely nonlinear element. (a) Schematic plot of the nonlinear K vs linear $\frac{1}{2L}$ landscape of inductive superconducting elements with centrosymmetric potentials. The Quarton forms a basis for this space along with the inductor. (b) Schematic line scale of the relative strength of nonlinear K of the elements in (a). The Quarton (represented by the spider symbol) defines the infinity limit of this scale. Corresponding potential landscapes are plotted below different elements to visually display the degree of anharmonicity / nonlinearity.

In this chapter, we provide a new insightful derivation of the Quarton that will highlight its importance in relation to all other nonlinear elements in cQED.

We start by introducing a plot of the nonlinear vs linear energy for inductive superconducting elements with centrosymmetric potentials (Fig. 3-1a). Note that the nonlinear $d^4U/d\phi^4$ is proportional to the Kerr coefficient (K) and the linear $d^2U/d\phi^2$ is inversely proportional to the inductance L (as was shown in the previous chapter). In general, the vectors specify a line representing the family of circuit elements achievable by varying E_J. We begin by finding the JJ at the bottom right of the plane with a relatively flat slope indicative of its relatively small nonlinearity. The $|\frac{d^4U}{d\phi^4}/\frac{d^2U}{d\phi^2}|$ is also plotted in Fig. 3-1b for ease of comparison. Note that other effectively single JJ qubits such as the transmon would also live on the JJ line.

We consider three possible techniques here for changing the nonlinearity versus linearity:

(1) add more JJs in series to decrease the relative nonlinearity,

(2) thread half a flux quantum ($\Phi_0/2$) of external magnetic flux through a loop of elements,

(3) connect elements in parallel to add their vectors on the plane.

For (1) with n identical JJs in series (all with $E_J \gg E_C$), phase ϕ across the chain of JJs is divided evenly across each JJ ($\phi \to \phi/n$) [29] which by Eqn.(2.21) implies that: $\frac{1}{L} \to \frac{1}{L}\frac{1}{n^2}, K \to K\frac{1}{n^4}$ so more JJs in series leads to a lower $|\frac{d^4U}{d\phi^4}/\frac{d^2U}{d\phi^2}|$ as shown in Fig. 1. In the limit that the number of series JJ $n \to \infty$, we get a superinductor [29], which is purely linear.

We can also (2) add a sweet spot flux bias $\Phi_0/2$. As discussed in the previous chapter, this flips the closure branch JJ vector to the top left of the plane of Fig. 1a because the external flux essentially shifts the cosine potential $U_{JJ}(\phi)$ via $\phi \to \phi + \pi$ and leaves a new $-U_{JJ}(\phi)$.

We can further using (3) to add vectors to produce flux qubits that live in the space between the flux-biased and unbiased JJ / SQUIDs. The top right corner of Fig. 3-1a shows the simplest flux qubit with two identical junctions with E_J in series in one arm, and a smaller junction with αE_J in the other arm. Recall from the previous

chapter that we are free to choose to let the external flux bias any branch of the flux qubit [47]. So without loss of generality, we choose for convenience the smaller junction to be the closure branch. Then, we see that one arm (spanning tree) of the flux qubit lives on the bottom right quadrant and the other (closure branch) lives up on the top left quadrant. Because the two arms don't have the same $|\frac{d^4U}{d\phi^4}/\frac{d^2U}{d\phi^2}|$ (Fig. 3-1b), when joined in parallel, the resulting flux qubit vector from the addition of the two arms can have different directions on the plane depending on the α value. Flux qubits with more junctions follow the same principle, with potential:

$$U(\phi) = nE_J \cos(\phi) + \alpha E_J \cos(\phi - \pi) \tag{3.3}$$

where n, the number of series JJs, can be larger than 2.

The Quarton is the special flux qubit with $\alpha = 0.5$ (or for general n, $\alpha = \frac{1}{n}$), at which point the negative inductance from the top left arm exactly cancels the positive inductance from the bottom right arm while the stronger postive K of the top left survives the addition to produce a purely nonlinear element. Physically, it means that the two branches of positive and negative linear inductances completely destructively interfere, and thus linearly behave as an infinite inductance inductor (open circuit). From its position on the plane, it is immediately clear that the Quarton is a basis vector along with the inductor. In Fig. 3-1b, the Quarton defines the infinity end of the $|\frac{d^4U}{d\phi^4}/\frac{d^2U}{d\phi^2}|$ scale as the polar opposite of the linear inductor which defines the zero point. This is also graphically illustrated by the potential diagrams beneath the scale, showing maximally anharmonic behavior for the Quarton. Examining Fig. 3-1a, we see that by simply adding the Quarton in parallel, we can add the Quarton vector to any circuit element vector to selectively modify its nonlinearity without disturbing its linear behaviour.

3.1.1 Generality of derivation and unfavorable regimes

Recall from Chapter 2 that gauge freedom implies that our convenient choice of spanning tree and closure branch does not suffer any loss of generality. It immediately

follows that our geometric derivation in Fig. 3-1a is *general* and thus within the assumptions of the derivation, the grey region under the JJ line is not accessible. This means that flux qubits and other elements resulting from flux bias and series JJs cannot be used to produce a more negatively nonlinear superconducting element. In other words, *there is no negative Quarton within our framework.*

At first glance, it is surprising that Fig. 3-1 is not symmetric about the origin. However, there is a simple and intuitive stability argument for this. Recall from Chapter 2 that superconducting qubit and resonator systems are exactly analogous to nonlinear spring-mass systems. Therefore, we can lean on the classical intuition that a mass cannot be stable in a concave potential function such as that of a negative Quarton. As for bottom right regions of Fig. 3-1a with negative quartic but positive quadratic potential, by simply examining large ϕ behavior and invoking periodicity of the potential function, we can see that these potential functions have deep global minimums at $\phi \neq 0$. Therefore, these systems will also be energetically unstable and tend to absorb or emit a flux quantum (i.e. shift ϕ) to relax into the true ground state.

3.1.2 Nonlinear optics language: $\chi^{(1)}, \chi^{(3)}$ of qubits

This is a good place to pause and summarize everything we discussed so far in the language of nonlinear optics. Superconducting qubits derive their nonlinearity from the nonlinear potential of the JJ, which can be seen as a nonlinear magnetic element. This is exactly analogous with usual atoms that derive their nonlinearity from the nonlinear potential of the atomic electric field. Therefore, borrowing the classification of nonlinear optical materials by their nonlinear electrical susceptibility $\chi^{(3)}$, we can analogously express superconducting qubit properties in terms of their nonlinear magnetic susceptibility:

$$\chi_m = \mu_r - 1 = \chi_m^{(1)} + \chi_m^{(3)} H^2 \tag{3.4}$$

To make the analogy more exact, we can invoke the duality symmetry for electromagnetic waves [1]. Briefly, this is the symmetry between electric and magnetic fields in source-free Maxwell's equations. By Noether's Theorem, there is an associated conserved quantity (helicity) which essentially locks the relative magnitude of E and H fields in vacuum. This can be generalized to materials by applying the constitutive relations via the transformation $E \rightarrow \sqrt{\frac{\epsilon}{\mu}}E$ [1]. Therefore, a strongly magnetic ($\mu \rightarrow \infty$) material can be seen as an epsilon-near-zero (ENZ) $\epsilon \rightarrow 0$ medium.

The nonlinear optics language allows us to succinctly capture the power of engineered nonlinear atoms. Using $\epsilon \xleftrightarrow{\text{duality}} \frac{1}{\mu}$, we see that the magnetic linear and nonlinear axes of Fig. 3-1a can be seen as being related to the familiar electric $\chi^{(1)}$ and $\chi^{(3)}$ of nonlinear optics. Then, the effect of varying α in Fig. 3-1a can really be seen as varying nonlinearity $\chi^{(3)}$. Remarkably, we can easily access regions of both positive and negative $\chi^{(3)}$, which is extremely convenient for many applications. For instance, one can pick a nonlinearity of the opposite sign to material dispersion to support solitons in both regions of normal and anomalous disperison. Another example would be quasi-phase matching using alternating regions with opposite signs of nonlinearity [5].

For the Quarton which has $\mu \rightarrow \infty$, we can see it as having $\epsilon \rightarrow 0$ or equivalently $\chi^{(1)} \rightarrow -1$. This is also valid in practice, as the infinite linear inductance of the Quarton represents an electric open – which is equivalent to a zero capacitance capacitor. In summary, the Quarton's trivial linear properties and non-zero $\chi^{(3)}$ makes it a "plug-and-play" source of nonlinearity that can be added to materials to edit nonlinearity at will without impacting the linear properties.

3.2 Note on junction capacitance

We have neglected all capacitances in the derivations of this chapter. However, all JJs have an (typically small, femtofarad level) intrinsic junction capacitance between the superconducting electrodes. This can be modelled as a parallel capacitor to the JJ. When we use the Quarton as a coupler, this small junction capacitance introduces

linear capacitive coupling g_c of the opposite sign to linear inductive coupling g_l [31]. This would be detrimental to achieving a purely nonlinear coupling, which is the subject of the next Chapter.

However, because g_c and g_l have opposite signs. It has been shown [31, 24] that the linear effect of the non-ideal capacitance can be exactly cancelled by a linear inductance when:

$$|g_c| = |g_l|. \tag{3.5}$$

Therefore, it is a subtle but important point that we will often want to design the Quarton to have a small amount of linear inductive energy to cancel its own small intrinsic junction capactive energy. Geometrically, this amounts to "tilting" the Quarton vector slightly to the right in Fig. 3-1a.

As such, in this and the following chapters, we will largely forgo the discussion about junction capacitances and deal only with "tilted" Quartons that introduce no linear coupling.

Chapter 4

The Quarton as a nonlinear coupler

4.1 Literature on circuit QED light-matter coupling

The field of circuit QED (cQED) studies the light-matter coupling between (linear) microwave photons and (nonlinear) superconducting qubits. Notice how our definition of "light" and "matter" intimately relates to the nonlinearity of the element under study, this will be the main theme of this Chapter – how we can use nonlinearity engineering to seamlessly transition between the nonlinear and the linear, and thus between the atomic and the photonic.

Typically, light-matter coupling is *linear* and takes the well known Jaynes-Cummings form [4], where single excitations are coherently exchanged between atomic (σ_z) and photonic modes ($\hat{a}$):

$$H = \hbar\omega_{\mathrm{r}}\left(a^{\dagger}a + \frac{1}{2}\right) + \frac{\hbar\Omega}{2}\sigma^{z} + \hbar g\left(a^{\dagger}\sigma^{-} + \sigma^{+}a\right) \tag{4.1}$$

This *linear* coupling causes mixing of the atomic and photonic modes, with both modes becoming "dressed" and the eigenmodes take on both nonlinear atomic and linear photonic characteristics. Because of the nonlinearity of the qubit, in the dispersive limits (high frequency detuning between qubit and photon modes) [14], the Jaynes-Cummings linear coupling can exhibit an effective nonlinear coupling between

atomic and photonic modes $\frac{g^2}{\Delta}\sigma^z a^\dagger a$:

$$H' = \hbar\left[\omega_{\rm r} + \frac{g^2}{\Delta}\sigma^z\right] a^\dagger a + \frac{\hbar}{2}\left[\Omega + \frac{g^2}{\Delta}\right]\sigma^z. \tag{4.2}$$

Note in the transformed Hamiltonian H' above, we have neglected the fact that the photon mode also inherits some small of the nonlinearity of the atom [4]. However, this inherited nonlinearity is important as it sets the critical number $n_{crit} = \frac{\Delta^2}{4g^2}$ of photons in the cavity for important applications such as readout, gates, and bosonic qubit fidelities [37].

The AC Stark shift $\frac{g^2}{\Delta}\sigma^z a^\dagger a$ is extremely important for quantum information processing. Its QND (quantum-non-demolition) nature allows for non-destructive readout of qubit or photon states [4], and is exploited in almost all single and two-qubit gates [37, 36]. However, it is weak (typically of order 10-100 megahertz) because it is ultimately a linear coupling dressed by the nonlinear nature of the qubit – and so the linear g cannot be made large without significant overlap in the atomic and photonic modes which lower n_{crit} and degrades Purcell filtering [11].

We can again use the language of nonlinear optics for some additional insights. The AC Stark shift $\frac{g^2}{\Delta}\sigma^z a^\dagger a$ is a third-order nonlinear term. This is more obvious if we recall (Eqn. 2.25) that our qubits are only slightly anharmonic oscillators and in the limit that $E_C(K) \to 0$ we get that $\frac{\Omega}{2}\sigma^z \to \Omega\hat{b}^\dagger\hat{b}$ and the cross-Kerr is clearly due to four-wave mixing: $g_{ab}\hat{b}^\dagger\hat{b}a^\dagger a$. Similarly, another important interaction in cQED – the longitudinal coupling of two qubits [25] of the form $g_{zz}\sigma_{z,a}\sigma_{z,b}$ can also be seen as nonlinear four-wave mixing in the other limit that the linear photon mode picks up some non-zero Kerr.

The cross-Kerr $g_{ab}\hat{b}^\dagger\hat{b}a^\dagger a$ interaction is extremely important as it is an effective photon-photon interaction. It is exploited in QND photon detection [39, 15], photon-based quantum computation [41, 42], and can be used to make exotic photonic molcules and photonic matter [20].

The longitudinal qubit interaction, an effective matter-matter coupling, is also critical for implementing two-qubit gates [38], quantum annealing schemes [27], and

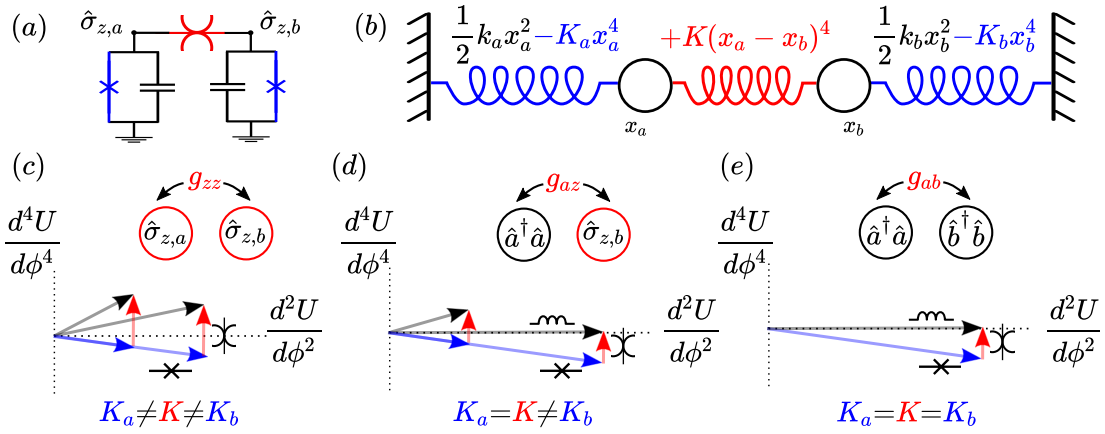

Figure 4-1: Nonlinearity engineering of light-matter interactions. (a) Circuit of Quarton nonlinearly coupling two qubits. (b) An exact spring-mass analog of (a). (c) Quarton enhancing nonlinearity of qubits, facilitates longitudinal qubit-qubit coupling. (d) Quarton eliminating nonlinearity of one qubit, facilitates effective AC-Stark like qubit-photon coupling. (e) Quarton eliminating nonlinearity of both qubits, facilitates effective cross-Kerr photon-photon coupling. $\hat{a}, b$ represent annihilation operators for photon modes, σ_z represents qubit modes.

single photon transistor [31].

4.2 Erasing and enhancing nonlinearity

All these important interactions in cQED all rely on nonlinearity. Indeed, linear coupling of linear systems can be trivially diagonalized and cannot be useful for quantum computation [14]. Therefore, we should expect that the maximally nonlinear properties of the Quarton can offer new tools for cQED. Indeed, we will show hereafter that the Quarton can be used to erase and enhance nonlinearity.

Consider the elementary circuit of two qubits (labelled a and b) coupled via a Quarton, shown in Fig. 4-1a. Using the mass-spring analogy we developed earlier, we can construct an exact analogy for the system (shown to four order in ϕ or x) in Fig. 4-1b. It is important to note that for any other coupling element, there would be some non-zero linear coupling (some extra $k(x_a - x_b)^2$ term in the red Quarton spring) which would severely degrade the performance, as we will show later.

Remarkably, by simply adjusting the relative magnitudes of the qubit Kerrs (K_a, K_b) to the coupling Quarton Kerr (K), we can access all three regimes of nonlinear cou-

pling. As shown in Fig. 4-1c,d,e, these regimes are longitudinal qubit-qubit coupling, AC Stark shift-like qubit-photon coupling, and cross-Kerr photon-photon coupling, respectively. Note that we use σ_z and $\hat{a}^\dagger\hat{a}, \hat{b}^\dagger\hat{b}$ to denote qubit and photon modes, respectively.

This is because the Quarton's quartic potential leads to a purely nonlinear coupling potential of the form:

$$E_J(\phi_a - \phi_b)^4 \approx E_J(\phi_a^4 + \phi_b^4 - 6\phi_a^2\phi_b^2 + ...) \tag{4.3}$$

which has non-coupling nonlinear corrections ϕ_{ab}^4 to the qubit's nonlinearity. The leading order coupling term $\phi_a^2\phi_b^2$ is strictly a nonlinear cross-Kerr term. Therefore, we immediately see that a Quarton coupler leads to modification of mode nonlinearity and nonlinearly coupled linearly uncoupled modes. The modification of nonlinearity can thus turn matter-like qubit modes into light-like photon modes, and vice versa.

This can be intuitively represented on the linear-nonlinear diagram for each case. As shown in Fig. 4-1c, when the Quarton vector (drawn in red) does not cancel the JJ vector (drawn in blue), the resulting sum (drawn in black) is non-zero in the vertical nonlinear axis and thus represent residual resonator Kerr. This $K_a \neq K \neq K_b$ situation leaves us with two qubits longitudinally coupled.

In Fig. 4-1d, the Quarton vector (red) does cancel one of the JJ vectors (blue) but not the other. Thus, one of the resulting sums (black) is zero in the vertical nonlinear axis and represent a linear resonator; the other is non-zero and represents a nonlinear resonator or qubit. This $K_a = K \neq K_b$ situation leaves us with effective AC Stark shift between qubit and photon.

In Fig. 4-1e, the Quarton vector (red) cancels the two identical JJ vectors (blue). Thus, the resulting sums (black) are both zero in the vertical nonlinear axis and represent two linear resonator or photon modes. This $K_a = K = K_b$ situation leaves us with a remarkable system that is that exhibits *cross-Kerr without self-Kerr*.

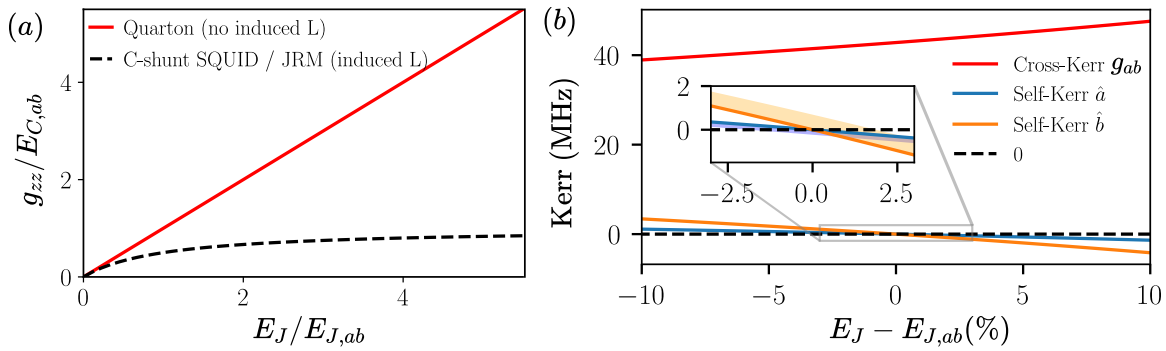

Figure 4-2: Quarton enabled coupling. (a) Strong longitudinal coupling of transmons showing $g_{zz} \gg E_C$. (b) Cross-Kerr coupling g_{ab} of resonators without self-Kerr.

4.3 Evaluating Quarton coupling

In Fig. 4-2, we evaluate the performance of the system in Fig.4-1. As we mentioned earlier, the absence of linear coupling in Quarton coupling is incredibly beneficial. In Fig. 4-2a, we see that the absence of linear coupling leads to a dramatic improvement in available coupling strength g_{zz} relative to qubit anharmonicity E_C. In the literature, nonlinear coupling via C-shunt SQUID [31] or JRM (Josephson Ring Modulator) [27] are limited to $g_{zz}/E_C \approx 1$ because the linear coupling that accompany nonlinear coupling in these systems reduce the zero point fluctuation ϕ_{ZPF} of qubits. Specifically, linear coupling changes $E_{J,ab}$ of qubits to an effective $E_J + E_{J,ab}$ (E_J is the Josephson energy of the coupler), and by extension the zero point fluctuation $\phi_{ZPF} = (2E_C/E_J)^{1/4}$ [14]. Reduced zero point fluctuation reduces the achievable coupling [31, 27]:

$$g_{zz} = E_C \frac{E_J}{\sqrt{E_{Ja} + E_J}\sqrt{E_{Jb} + E_J}} \tag{4.4}$$

Using the Quarton instead, we can avoid the detrimental linear coupling induced $E_J \to E_J + E_{J,ab}$, and achieve:

$$g_{zz} = E_C \frac{E_J}{\sqrt{E_{Ja}}\sqrt{E_{Jb}}} \tag{4.5}$$

See Appendix A for a detailed derivation of Eqn. 4.4 and Eqn. 4.5, as well as the fundamental limit on g_{zz}/E_C (Eqn. A.14).

In Fig. 4-2b, we numerically compute the cross-Kerr without self-Kerr corresponding to Fig.4-1e. Simulation is performed using QuCAT [12]. We see that as the effective E_J of the Quarton approaches that of the qubit JJ's ($E_{J,ab}$), we get ideal cross-Kerr g_{ab} with near zero self-Kerr. In the inset, we show the minor effect of residual linear coupling (shaded area) due to a small junction capacitance associated with the Quarton. The linear coupling shifts the zero Kerr points for the two modes in the opposite direction, so simultaneous self-Kerr cancellation of both modes can no longer be achieved by the Quarton.

This is clear if we consider that the linear coupling introduces some additional Jaynes-Cummings (J.C.) -like term into the otherwise ideal Hamiltonian:

$$H = \omega_a \hat{a}^\dagger \hat{a} + \omega_b \hat{b}^\dagger \hat{b} + \chi \hat{a}^\dagger \hat{a} \hat{b}^\dagger \hat{b} \tag{4.6}$$

$$\xrightarrow{J.C.} \omega_a \hat{a}^\dagger \hat{a} + \omega_b \hat{b}^\dagger \hat{b} + \chi \hat{a}^\dagger \hat{a} \hat{b}^\dagger \hat{b} + g(\hat{a}^\dagger \hat{b} + \hat{b}^\dagger \hat{a}) \tag{4.7}$$

which mixes the two modes a, b. We can diagonalize the J.C. part to get eigenmodes $\tilde{a}, \tilde{b}$ which will be some superposition of the original a, b modes:

$$a = \xi \tilde{a} + \eta \tilde{b} \tag{4.8}$$

$$b = \eta \tilde{a} - \xi \tilde{b} \tag{4.9}$$

And we see that this diagonalization turns the cross-Kerr term into:

$$\chi \hat{a}^\dagger \hat{a} \hat{b}^\dagger \hat{b} \rightarrow \chi (\xi \tilde{a} + \eta \tilde{b})^\dagger (\xi \tilde{a} + \eta \tilde{b})(\eta \tilde{a} - \xi \tilde{b})^\dagger (\eta \tilde{a} - \xi \tilde{b}) \tag{4.10}$$

which re-introduces self-Kerr terms $\tilde{a}^{\dagger 2} \tilde{a}^2$ and $\tilde{b}^{\dagger 2} \tilde{b}^2$ into what was a purely cross-Kerr interaction.

As we discussed at the end of last chapter, this effect can be cancelled by using a "tilted" Quarton with the right amount of inductive energy that cancels the capacitive coupling energy.

Chapter 5

Quarton for traveling wave single photon detection

5.1 Literature review on photon detection

Working in the microwave frequencies has been a significant advantage for circuit QED [16]. Large microwave wavelengths means conventional microfabrication tools can relatively easily produce waveguides that serve as high-quality, low mode volume resonators [4], as well as photonic crystals [18] and metamaterials [6].

However, there is one glaring disadvantage to working with microwaves rather than optical wavelengths: The lack of reliable single photon detection [16]. Because a microwave photon have 10^{-5} times less energy than an optical photon, microwave single photon detection has proved difficult. Yet, reliable single photon detection is crucial for applications such as quantum communication [30], quantum sensing [3], modular and photon based quantum computing [32, 43], and even dark matter axion detection [26].

In the past decade, significant progress has been made. For instance, in 2010, Johnson et. al. [21] demonstrated QND detection of localized microwave photons in cavities. In 2011, Chen et. al. [8] showed destructive detection of traveling photons. In 2018, Kono et. al. [23] achieved high fidelity time-gated QND detection of traveling photons. However, an ideal detector similar in performance to the best

optical photon detectors [17] has remained elusive. Such a detector should offers high-fidelity, unconditional (not time-gated), non-destructive (ideally QND), broadband and photon-number resolving detection of traveling (itinerant) microwave photons [17].

Most existing single microwave photon detectors involve resonant cavities that trap photons and non-linearly couple them to read-out [23]. As such, these conventional single microwave photon detectors have a limited bandwidth-efficiency product because they suffer from the intrinsic interaction time versus bandwidth trade-off of the resonant cavities [39]. This well-known problem has an analog in resonator-based parametric amplifiers (e.g. the JPA [48]), wherein a narrow-band cavity is needed to trap the incident waves for the long amplification duration. Traveling wave devices like the Josephson Traveling Wave Parametric Amplifier (JTWPA) [28] circumvent this problem by replacing the resonant cavity with a long nonlinear transmission line in which the incident wave is amplified during travel. The instantaneous amplification bandwidth can be engineered to be many gigahertz, allowing for simultaneous multiplexed readout of many qubits.

We consider the design of a traveling wave version of single microwave photon detectors. In fact, in the optical domain, traveling wave photon detectors (TWPDs) [13] are already widely used for their high bandwidth-efficiency performance, which is required for receiving the high data-rate of current optical communication protocols. Recently, we collaborated in the proposal for a Josephson Traveling Wave Photon Detector (JTWPD) [15] which serves as a similarly high bandwidth-efficiency photon detector in the microwave regime, with the added benefit of non-destructive counting of single photon sensitivity. Because of the JTWPD's high bandwidth-efficiency performance, a well-designed JTWPD with a several hundred Megahertz bandwidth is theorized to have detection fidelity of $>99\%$ [15].

In this chapter, we build on our recent collaboration in [15] and propose an experimentally realizable Quarton based JTWPD.

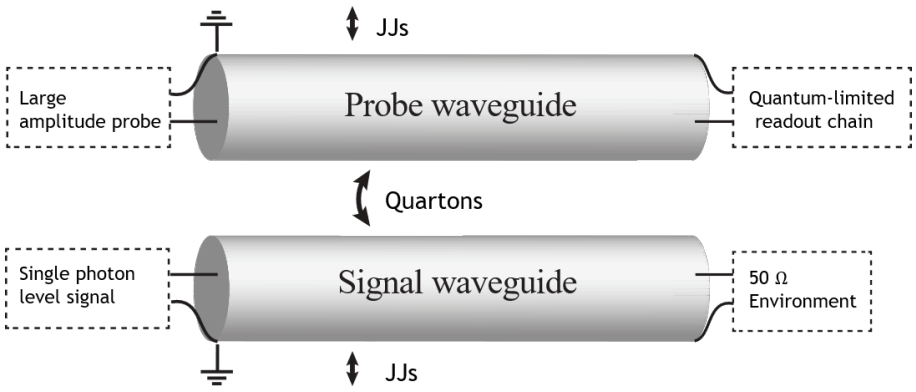

Figure 5-1: Schematic of a Quarton based JTWPD. Both probe and signal waveguides are linear (no self-Kerr) but there is nonlinear coupling (cross-Kerr) between them.

5.2 Quarton for JTWPD

Our quarton based JTWPD setup (Fig. 5-1) can be succintly summarized as follows: We design two nonlinearly coupled linearly uncoupled linear waveguides using (in part) as unit cell the circuit introduced in the previous chapter. We use one waveguide for signal and one waveguid for probe photons. We send a large number of probe photons to measure the single-photon level signal. The cross-Kerr interaction between the two waveguides causes a phase shift on the probe photons dependent on the signal photon number, which can be readout from a quantum-limited readout chain [28].

5.2.1 Multimodes: the Quarton coupled waveguides

Previously, we showed that the Quarton can engineer the nonlinearity of single-mode qubits and resonators. Here, we extend the results to multimode waveguides.

We will use the circuit (Fig. 4-1a) introduced in the previous chapter as part of the unit cell of the coupled waveguides. The circuit is drawn in Fig. 5-2 and represents Quarton coupling of two predominantly left-handed metamaterials with higher frequency cut-offs.

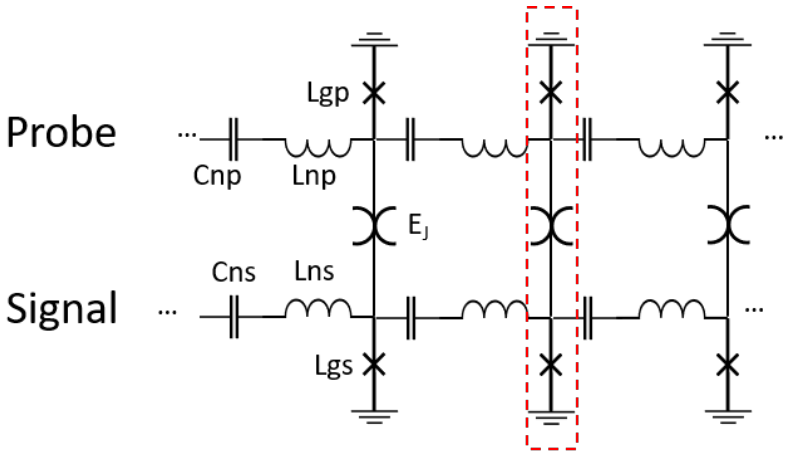

Figure 5-2: JTWPD circuit consisting of Quarton coupled of left-handed metamaterials with higher frequency cut-offs. Red box outlines the cross-Kerr without self-Kerr circuit shown in Fig. 4-1a, here the JJ acts as an effective inductor.

Broadband self-Kerr cancellation

Here, we provide a simple intuitive explanation for the nonlinear behavior of the system (red box in Fig. 5-2).

Let the superconducting phase in the probe and signal line be ϕ_p and ϕ_s, respectively. For a particular unit cell, the potential term U in the Lagrangian can be written (to 4th order in ϕ) as:

$$U = E_{Jp}(\phi_p^2/2 - \phi_p^4/24) + E_{Js}(\phi_s^2/2 - \phi_s^4/24) + E_J(\phi_s - \phi_p)^4/24 \tag{5.1}$$

where we used the Josephson energies E_{Jp}, E_{Js} corresponding to the linear inductance L_{gp}, L_{gs} labelled in Fig. 5-2. Expanding the Quarton's quartic potential, we can see that if:

$$E_{J,p} = E_{J,s} = E_J, \tag{5.2}$$

exactly the same condition as self-Kerr cancellation in Fig. 4-1e, all self-nonlinear terms $\phi_{s,p}^4$ in both lines cancel. We have not assumed any frequencies in this derivation thus far, and therefore this self-Kerr cancellation is *broadband*.

Because all other elements in the unit cell are linear, we are left with two *linear* waveguides *nonlinearly coupled*. Following Eqn. 4.3, we see that the leading order

nonlinear coupling is a cross-Kerr interaction. (We will discuss in the next section why the other nonlinear coupling terms are strongly suppressed.) Therefore, we have extended the single mode cross-Kerr without self-Kerr results from the previous chapter to multimode waveguides.

(It is easy to show that any self-Kerr in the probe waveguide will cause self-phase modulation which is much stronger than the cross-phase modulation signal. So the elimination of self-Kerr is essential to achieving high signal-to-noise and thus high efficiency photon detection.)

Note that in practice, it will be difficult to choose identical $L_{gs} = L_{gp}$ without sacrificing the ideal band structure. However, we can apply the insights from Chapter 3 (Fig.3-1a) and use different number of series JJ for L_{gs} and L_{gp}. As long as the Kerr nonlinearities of both ground nonlinear elements match the opposite sign Kerr nonlinearity induced by the Quarton, the self-Kerr cancellation will hold.

5.2.2 Metamaterial design

The particular construction of two left-handed metamaterials with high-frequency cutoff is chosen for two reasons. First, to engineer an appropriate passband in the two materials; and second, to minimize dark counts due to thermal photons.

Disjoint passbands

Recall from Chapter 2 that a left-handed metamaterial has a low frequency cut-off ω_{cL}:

$$\omega_{cL} \approx \frac{1}{\sqrt{C_n L_g}}. \tag{5.3}$$

By including the additional series inductors L_n, we include a high frequency cut-off ω_{cH} at about:

$$\omega_{cH} \approx \frac{1}{\sqrt{C_n L_n}} \tag{5.4}$$

where the series LC circuit hits resonance and approaches an electrical short with zero impedance. Therefore, by appropriate choice of circuit parameters, we can design a passband of several gigahertz between ω_{cL} and ω_{cH} given by Eqn. 5.3 and Eqn. 5.4.

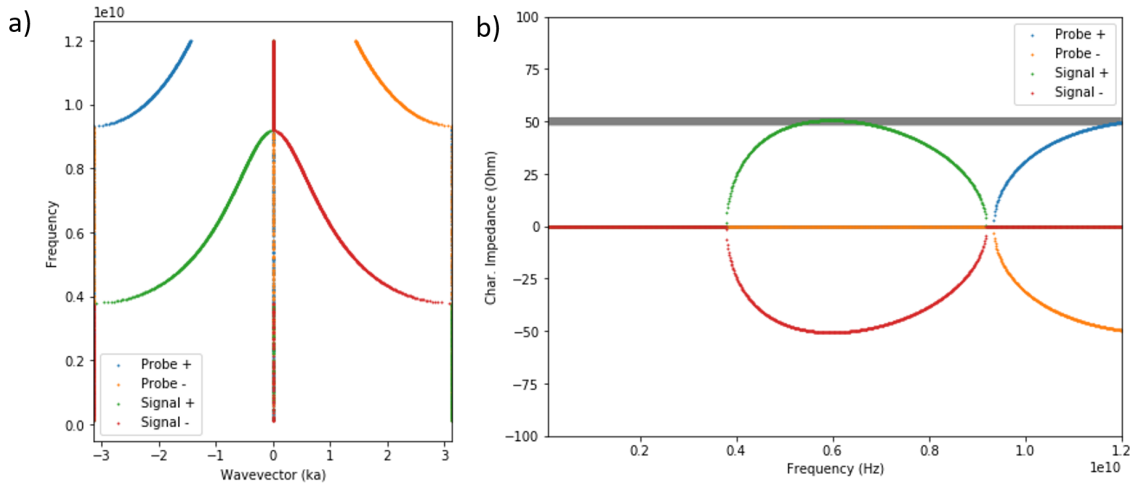

Figure 5-3: Linear JTWPD metamaterial properties calculated from ABCD matrices. a) Band structure b) Characteristic impedance Z_0 (grey region highlights impedance matched to $50 \pm 2\Omega$). Clear disjoint passpands and $Z_0 \to 0$ cut-off behavior shown. ('+' and '-' represent right and left moving eigensolutions.)

We take special care to make the signal and probe passbands disjoint (i.e. ω_{cH} of one waveguide is less than ω_{cL} of the other). This will strongly suppress the non-ideal Quarton coupling terms of the form:

$$E_J(\hat{a}^\dagger \hat{a} \hat{a} \hat{b}^\dagger + \hat{b}^\dagger \hat{b} \hat{b} \hat{a}^\dagger) + H.c.. \tag{5.5}$$

These terms can be viewed as correlated or stimulated hopping of photons between the waveguides [24]. If neglected, this can cause significant leakage of probe photons into the signal waveguide and destroy the detection process. With disjoint passbands, there are no common frequency modes between the two waveguides for photons to hop to. Photon hopping would then be energy non-conserving and thus highly suppressed.

Note that in practice, the L_n necessary for disjoint passbands is of order nH and thus JJs should be used in place of geometric inductors. The nonlinearity of these series JJs can be minimized by joining many JJs in series (Fig. 3-1a).

Solving the linear parts of the coupled waveguide in Fig.5-2 with the ABCD matrix formalism introduced in Chapter 2, we verify the two disjoint passbands shown in Fig. 5-3. The sample parameters chosen for the calculation are as follows: $L_{gs} =$

1.425nH, C_{ns} = 250fF, L_{ns} = 1.2nH, L_{gp} = 0.594nH, C_{np} = 83.3fF, L_{np} = 0.95nH. Note that a broad frequency band (5-7 GHz) of the signal waveguide is impedance matched to 50Ω for ease of integration with electronics.

Thermal photon and $Z_0 \to 0$ limits

Low frequency thermal photons are generated both within the JTWPD and enters the JTWPD through the 50 Ω environemnt. These thermal populations also cause cross-Kerr phase shift on the probe and thus lead to dark counts and noise.

To minimize the influence of thermal photons, we want the $Z_0 \to 0$ outside the intended detection frequency band of $5 - 7$ GHz. As we discussed in Chapter 2, the phase zero point fluctuation of modes is proportional to the characteristic impedance Z_0 [15]:

$$\phi_{ZPF}(\omega) \propto \sqrt{Z_0(\omega)} \tag{5.6}$$

Therefore, cross-Kerr coupling (which scales with ϕ_{ZPF}) is highly suppressed for frequency ranges with $Z_0 \to 0$. Because thermal photon population increases exponentially with lower frequency modes, the low frequency cut-off ω_{cL} is necessary to avoid detector saturation from thermal photons.

A primary motivation for our metamaterial design is to incorporate low frequency cut-off ω_{cL} and avoiding any diverging impedances $Z_0 \to \infty$. As shown in Fig. 5-3, every single cut-off in our metamaterial design follows the ideal limit $Z_0 \to 0$. Some other metamaterial design, e.g. right-handed waveguide with inductor to ground, will also provide ω_{cL}. Yet this cutoff results from an infinite impedance ground LC resonance. This $Z_0 \to \infty$ is ill-behaved and would cause any thermal photon population near ω_{cL} to overwhelm the cross-Kerr interaction and thus drown out the signal. Similarly, a CRLH metamaterial would have $Z_0 \to \infty$ at a similar resonant cutoff unless it is perfectly balanced (which is experimentally challenging). The left-handed metamaterial we designed involves similar experimental parameters to references like [45] and is therefore readily experimentally realizable.

Another benefit of $Z_0 \neq 50\Omega$ impedance mismatch at cut-offs is the formation of

cavity modes. Near cut-off frequencies, the strong reflection between the waveguide and the 50Ω environment creates cavity modes. Therefore, as long as the frequencies near cut-off are off-resonant with the cavity, they will be strongly suppressed.

Chapter 6

Conclusion

6.1 Summary

We provided a new derivation for the Quarton as a maximally nonlinear superconducting element. As part of this derivation, we introduced a convenient representation of cQED elements on a linear-nonlinear plane spanned by the Quarton and the linear inductor. Our derivation covers large classes of elements and highlights the higher nonlinearities achievable in positive, rather than traditionally negative, Kerr medium.

We used these results to perform nonlinearity engineering. We showed that the Quarton as a nonlinear coupler can amplify or erase nonlinearity of modes, causing them to behave more atomic or more photonic like. This allows us to reach novel regimes of light-matter interactions including much stronger longitudinal qubit coupling, and nonlinearly coupled linearly uncoupled linear modes.

Finally, we provided a detailed application example by designing coupled metamaterials that utilize Quarton coupling properties for an experimentally realizable Josephson traveling wave photon detector (JTWPD). The design involves two metamaterials that are cross-Kerr coupled but exhibit no self-Kerr nonlinearity.

We see great potential in the convenient "plug-and-play" nature of the Quarton for selective editting of nonlinear properties of artifical atoms and metamaterials. The nonlinearity engineering techique should provide both new insights and perspectives as well as serve as a powerful tool for the design of new circuit QED systems.

Appendix A

Derivation of Quarton enhanced longitudinal qubit coupling g_{zz}

A.1 Literature - coupling with linear L

We will provide a quick summary of the derivations of two relevant works in the literature, one using C-shunt SQUID [31] and one using JRM [27] for longitudinal g_{zz} coupling without linear coupling.

For C-shunt SQUID circuit [31] shown in Fig. A-1, the Lagrangian of only the C-shunt SQUID coupled qubits can be written as follows:

$$\begin{aligned}\mathcal{L} = &\frac{C_{J1}}{2}\dot{\varphi}_1^2 + \frac{C_{J2}}{2}\dot{\varphi}_2^2 + \frac{C_m}{2}\left(\dot{\varphi}_1 - \dot{\varphi}_2\right)^2 \\ &+ E_{J1}\cos\left(\frac{\varphi_1}{\varphi_0}\right) + E_{J2}\cos\left(\frac{\varphi_2}{\varphi_0}\right) + E_{Jm}\cos\left(\frac{\varphi_1 - \varphi_2}{\varphi_0}\right)\end{aligned} \tag{A.1}$$

Expanding the SQUID cosine potential to order φ^4, we see that:

$$E_{Jm}\cos\left(\frac{\varphi_1 - \varphi_2}{\varphi_0}\right) \approx -E_{Jm}[(\frac{\varphi_1 - \varphi_2}{\varphi_0})^2/2 - (\frac{\varphi_1 + \varphi_2}{\varphi_0})^4/24]. \tag{A.2}$$

in which the linear inductance part:

$$-E_{Jm}(\frac{\varphi_1 - \varphi_2}{\varphi_0})^2/2 = -\frac{E_{Jm}}{2}[(\frac{\varphi_1}{\varphi_0})^2 + (\frac{\varphi_2}{\varphi_0})^2 - \frac{2\varphi_1\varphi_2}{\varphi_0})]. \tag{A.3}$$

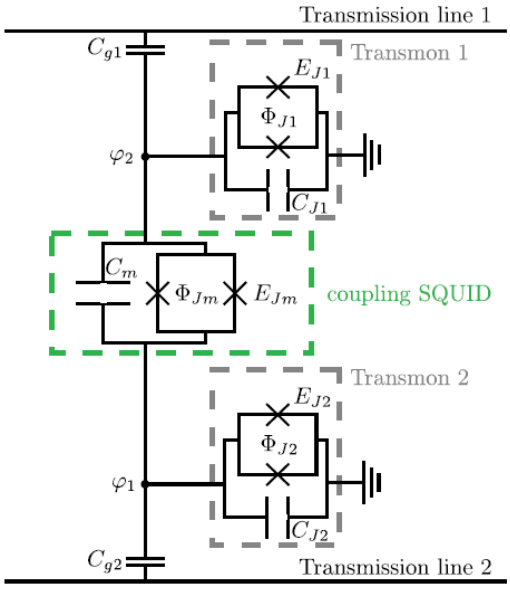

Figure A-1: C-shunt SQUID (green) nonlinearly coupling two transmons (grey) [31]

The last term provides linear inductive coupling (which will be cancelled by an opposite signed capacitive linear coupling). However, the first two terms are not coupling terms but rather cause a change in effective inductance of the qubits. From Eqn.A.1, expanding the qubit $E_{J,12}$ cosine terms and collecting coefficients, we find the SQUID E_{Jm} changes $E_{J,12}$ of qubits to an effective $E_J + E_{J,12}$.

The lowering of qubit effective inductance causes a lowering of characteristic impedance and thus the qubit zero point fluctuation $\varphi_{ZPF,12} = (2E_{C,12}/E_{J,12})^{1/4}$ [14] is lowered:

$$\varphi_{ZPF,12} = [\frac{2E_{C,12}}{(E_J + E_{J,12})}]^{1/4} \tag{A.4}$$

The longitudinal coupling strength g_{zz} scales with both coupling E_{Jm} and the amplitude of the qubits (given by φ_{ZPF}):

$$g_{zz} \propto E_{Jm}\varphi^2_{ZPF,1}\varphi^2_{ZPF,2} \tag{A.5}$$

$$\propto \sqrt{E_{C,1}E_{C,2}}\frac{E_{Jm}}{\sqrt{E_{J1}+E_{Jm}}\sqrt{E_{J2}+E_{Jm}}} \tag{A.6}$$

Assuming the same E_C for both qubits for simplicity (E_C is relatively fixed for transmons [22]), we obtain the Eqn. 4.4 expression in Chapter 4.

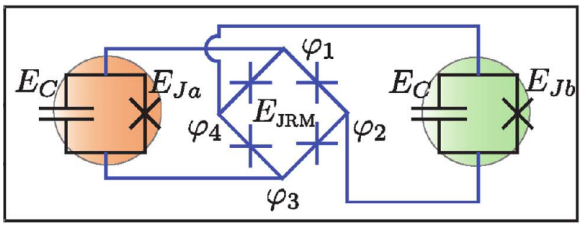

Figure A-2: JRM facilitated longitudinal qubit coupling g_{zz} [27].

The derivation is similar for JRM (shown in Fig. A-2) [27], which has an ideal coupling potential (for modes labelled a, b):

$$4E_{\mathrm{JRM}} \cos\left(\frac{\phi_a}{2}\right) \cos\left(\frac{\phi_b}{2}\right) \tag{A.7}$$

$$\approx 4E_{\mathrm{JRM}}(1 - \frac{1}{2}(\frac{\phi_a}{2})^2 + ...)(1 - \frac{1}{2}(\frac{\phi_b}{2})^2 + ...) \tag{A.8}$$

Similar to C-shunt SQUID, we see that the JRM introduces non-coupling inductive terms $\phi_{a,b}^2$ which modify the inductance of the qubits. The rest follows straightforwardly from the C-shunt SQUID, and we get the same Eqn. 4.4 expression in Chapter 4.

We see that any coupling element with linear inductance will lower the qubit inductance. This can bee explained in terms of an equivalent circuit model. When connected to a coupling element with linear inductance, the qubit will see an effective parallel inductor which lowers its own inductance. Therefore, none of these schemes can facilitate strong longitudinal $g_{zz} \gg E_C$.

A.2 Quarton coupler - coupling without linear L

When we couple with a Quarton which is linearly an electrical open circuit, the qubits do not "see" any parallel linear inductance (it is linearly electrically isolated). It follows that the quartic coupling potential of the Quarton:

$$E_J(\varphi_a - \varphi_b)^4 \approx E_J(\varphi_a^4 + \varphi_b^4 + ...) \tag{A.9}$$

has noncoupling terms $\phi_{a,b}^4$ which only modifies the nonlinearity of the qubits. The quadratic noncoupling terms $\phi_{a,b}^2$ introduced by JRM and C-Shunt SQUID are completely absent. As a result, the inductance and thus the zero point fluctuation of the qubits are, to first order, unchanged. Therefore, we get

$$g_{zz} \propto E_{Jm}\varphi_{ZPF,1}^2\varphi_{ZPF,2}^2 \tag{A.10}$$

$$\propto \sqrt{E_{C,1}E_{C,2}}\frac{E_{Jm}}{\sqrt{E_{J1}}\sqrt{E_{J2}}} \tag{A.11}$$

corresponding to Eqn.4.5.

A.2.1 Fundamental $g_{zz} \gg E_C$ limit

Deep into the $g_{zz} \gg E_C$ limit, second order effects emerge and the Quarton's nonlinear modification of the qubit inductance also start to affect the qubit's zero point fluctuation.

We have neglected these second order effects thus far because they represent a fundamental limit to high g_{zz}. Even the most ideal purely g_{zz} interaction would incur such effects. Thus, they impose a tight bound on the highest possible g_{zz} achievable. Here, we provide a rough estimate of their influence.

We can write the Quarton's noncoupling corrections $E_J\phi_{a,b}^4$ as:

$$E_J\phi_{a,b}^4 \approx E_J\phi_{ZPF,ab}^2\phi_{a,b}^2 \tag{A.12}$$

which is valid when the qubits have low population. For typical transmons [22], we have:

$$\phi_{ZPF,ab}^2 \approx 0.1. \tag{A.13}$$

Therefore, Eqn.4.5 would be corrected with:

$$g_{zz} \approx E_C\frac{E_J}{\sqrt{E_{Ja}+0.1E_J}\sqrt{E_{Jb}}+0.1E_J}. \tag{A.14}$$

which would have little impact until we are deep in the regime of $g_{zz} \gg E_C$.

Bibliography

[1] David L Andrews. *Photonics, Volume 1: Fundamentals of Photonics and Physics*. John Wiley & Sons, 2015.

[2] Frank Arute, Kunal Arya, Ryan Babbush, Dave Bacon, Joseph C Bardin, Rami Barends, Rupak Biswas, Sergio Boixo, Fernando GSL Brandao, David A Buell, et al. Quantum supremacy using a programmable superconducting processor. *Nature*, 574(7779):505–510, 2019.

[3] S Barzanjeh, S Pirandola, D Vitali, and JM Fink. Experimental microwave quantum illumination. *arXiv preprint arXiv:1908.03058*, 2019.

[4] Alexandre Blais, Ren-Shou Huang, Andreas Wallraff, S. M. Girvin, and R. J. Schoelkopf. Cavity quantum electrodynamics for superconducting electrical circuits: An architecture for quantum computation. *Phys. Rev. A*, 69:062320, Jun 2004.

[5] Robert W Boyd. *Nonlinear optics*. Academic press, 2019.

[6] Christophe Caloz, Atsushi Sanada, and Tatsuo Itoh. A novel composite right-/left-handed coupled-line directional coupler with arbitrary coupling level and broad bandwidth. *IEEE Transactions on Microwave Theory and Techniques*, 52(3):980–992, 2004.

[7] Hongsheng Chen, Lixin Ran, Jiangtao Huangfu, Tomasz M Grzegorczyk, and Jin Au Kong. Equivalent circuit model for left-handed metamaterials. *Journal of applied physics*, 100(2):024915, 2006.

[8] Y-F Chen, D Hover, S Sendelbach, L Maurer, ST Merkel, EJ Pritchett, FK Wilhelm, and R McDermott. Microwave photon counter based on josephson junctions. *Physical review letters*, 107(21):217401, 2011.

[9] AA Clerk, KW Lehnert, P Bertet, JR Petta, and Y Nakamura. Hybrid quantum systems with circuit quantum electrodynamics. *Nature Physics*, pages 1–11, 2020.

[10] Michel H Devoret and Robert J Schoelkopf. Superconducting circuits for quantum information: an outlook. *Science*, 339(6124):1169–1174, 2013.

[11] Nicolas Didier, Jérôme Bourassa, and Alexandre Blais. Fast quantum nondemolition readout by parametric modulation of longitudinal qubit-oscillator interaction. *Physical review letters*, 115(20):203601, 2015.

[12] Mario F Gely and Gary A Steele. Qucat: quantum circuit analyzer tool in python. *New Journal of Physics*, 22(1):013025, 2020.

[13] Kirk Steven Giboney, Mark JW Rodwell, and John E Bowers. Traveling-wave photodetectors. *IEEE Photonics Technology Letters*, 4(12):1363–1365, 1992.

[14] Steven M Girvin. Superconducting qubits and circuits: Artificial atoms coupled to microwave photons. *Lectures delivered at Ecole d'Ete Les Houches*, 2011.

[15] A Grimsmo, B Royer, JM Kreikebaum, Y Ye, K O'Brien, I Siddiqi, and A Blais. Quantum metamaterial for nondestructive microwave photon counting. *arXiv preprint arXiv:2005.06483*, 2020.

[16] Xiu Gu, Anton Frisk Kockum, Adam Miranowicz, Yu-xi Liu, and Franco Nori. Microwave photonics with superconducting quantum circuits. *Physics Reports*, 718:1–102, 2017.

[17] Robert H Hadfield. Single-photon detectors for optical quantum information applications. *Nature photonics*, 3(12):696, 2009.

[18] PM Harrington, Mahdi Naghiloo, D Tan, and KW Murch. Bath engineering of a fluorescing artificial atom with a photonic crystal. *Physical Review A*, 99(5):052126, 2019.

[19] John David Jackson. Classical electrodynamics, 1999.

[20] Jiasen Jin, Davide Rossini, Rosario Fazio, Martin Leib, and Michael J Hartmann. Photon solid phases in driven arrays of nonlinearly coupled cavities. *Physical review letters*, 110(16):163605, 2013.

[21] BR Johnson, MD Reed, Andrew Addison Houck, DI Schuster, Lev S Bishop, Eran Ginossar, JM Gambetta, L DiCarlo, L Frunzio, SM Girvin, et al. Quantum nondemolition detection of single microwave photons in a circuit. *Nature Physics*, 6(9):663–667, 2010.

[22] Jens Koch, M Yu Terri, Jay Gambetta, Andrew A Houck, DI Schuster, J Majer, Alexandre Blais, Michel H Devoret, Steven M Girvin, and Robert J Schoelkopf. Charge-insensitive qubit design derived from the cooper pair box. *Physical Review A*, 76(4):042319, 2007.

[23] Shingo Kono, Kazuki Koshino, Yutaka Tabuchi, Atsushi Noguchi, and Yasunobu Nakamura. Quantum non-demolition detection of an itinerant microwave photon. *Nature Physics*, 14(6):546, 2018.

[24] Marios Kounalakis, Christian Dickel, Alessandro Bruno, Nathan K Langford, and Gary A Steele. Tuneable hopping and nonlinear cross-kerr interactions in a high-coherence superconducting circuit. *npj Quantum Information*, 4(1):1–7, 2018.

[25] Philip Krantz, Morten Kjaergaard, Fei Yan, Terry P Orlando, Simon Gustavsson, and William D Oliver. A quantum engineer's guide to superconducting qubits. *Applied Physics Reviews*, 6(2):021318, 2019.

[26] SK Lamoreaux, KA Van Bibber, KW Lehnert, and G Carosi. Analysis of single-photon and linear amplifier detectors for microwave cavity dark matter axion searches. *Physical Review D*, 88(3):035020, 2013.

[27] Martin Leib, Peter Zoller, and Wolfgang Lechner. A transmon quantum annealer: Decomposing many-body ising constraints into pair interactions. *Quantum Science and Technology*, 1(1):015008, 2016.

[28] Chris Macklin, K OâĂŹBrien, D Hover, ME Schwartz, V Bolkhovsky, X Zhang, WD Oliver, and I Siddiqi. A near–quantum-limited josephson traveling-wave parametric amplifier. *Science*, 350(6258):307–310, 2015.

[29] Nicholas A Masluk, Ioan M Pop, Archana Kamal, Zlatko K Minev, and Michel H Devoret. Microwave characterization of josephson junction arrays: Implementing a low loss superinductance. *Physical review letters*, 109(13):137002, 2012.

[30] Anirudh Narla, Shyam Shankar, Michael Hatridge, Zaki Leghtas, Katrina M Sliwa, Evan Zalys-Geller, Shantanu O Mundhada, Wolfgang Pfaff, Luigi Frunzio, Robert J Schoelkopf, et al. Robust concurrent remote entanglement between two superconducting qubits. *Physical Review X*, 6(3):031036, 2016.

[31] Lukas Neumeier, Martin Leib, and Michael J Hartmann. Single-photon transistor in circuit quantum electrodynamics. *Physical review letters*, 111(6):063601, 2013.

[32] Naomi H Nickerson, Joseph F Fitzsimons, and Simon C Benjamin. Freely scalable quantum technologies using cells of 5-to-50 qubits with very lossy and noisy photonic links. *Physical Review X*, 4(4):041041, 2014.

[33] Thomas Niemczyk, F Deppe, H Huebl, EP Menzel, F Hocke, MJ Schwarz, JJ Garcia-Ripoll, D Zueco, T Hümmer, E Solano, et al. Circuit quantum electrodynamics in the ultrastrong-coupling regime. *Nature Physics*, 6(10):772–776, 2010.

[34] Terry P Orlando and Kevin A Delin. *Foundations of applied superconductivity*, volume 8. Addison-Wesley Reading, MA, 1991.

[35] David M Pozar. *Microwave Engineering 3e*. Wiley, 2006.

[36] Shruti Puri and Alexandre Blais. High-fidelity resonator-induced phase gate with single-mode squeezing. *Physical review letters*, 116(18):180501, 2016.

[37] Serge Rosenblum, Yvonne Y Gao, Philip Reinhold, Chen Wang, Christopher J Axline, Luigi Frunzio, Steven M Girvin, Liang Jiang, Mazyar Mirrahimi, Michel H Devoret, et al. A cnot gate between multiphoton qubits encoded in two cavities. *Nature communications*, 9(1):1–6, 2018.

[38] Tanay Roy, Suman Kundu, Madhavi Chand, Sumeru Hazra, N Nehra, R Cosmic, A Ranadive, Meghan P Patankar, Kedar Damle, and R Vijay. Implementation of pairwise longitudinal coupling in a three-qubit superconducting circuit. *Physical Review Applied*, 7(5):054025, 2017.

[39] Baptiste Royer, Arne L Grimsmo, Alexandre Choquette-Poitevin, and Alexandre Blais. Itinerant microwave photon detector. *Physical review letters*, 120(20):203602, 2018.

[40] JA Schreier, Andrew A Houck, Jens Koch, David I Schuster, BR Johnson, JM Chow, Jay M Gambetta, J Majer, L Frunzio, Michel H Devoret, et al. Suppressing charge noise decoherence in superconducting charge qubits. *Physical Review B*, 77(18):180502, 2008.

[41] Jeffrey H Shapiro. Single-photon kerr nonlinearities do not help quantum computation. *Physical Review A*, 73(6):062305, 2006.

[42] Jeffrey H Shapiro and Mohsen Razavi. Continuous-time cross-phase modulation and quantum computation. *New Journal of Physics*, 9(1):16, 2007.

[43] Justin B Spring, Benjamin J Metcalf, Peter C Humphreys, W Steven Kolthammer, Xian-Min Jin, Marco Barbieri, Animesh Datta, Nicholas Thomas-Peter, Nathan K Langford, Dmytro Kundys, et al. Boson sampling on a photonic chip. *Science*, 339(6121):798–801, 2013.

[44] David H Staelin, Ann W Morgenthaler, and Jin Au Kong. *Electromagnetic waves*. Pearson Education India, 1994.

[45] H Wang, AP Zhuravel, S Indrajeet, Bruno G Taketani, MD Hutchings, Y Hao, F Rouxinol, FK Wilhelm, MD LaHaye, AV Ustinov, et al. Mode structure in superconducting metamaterial transmission-line resonators. *Physical Review Applied*, 11(5):054062, 2019.

[46] F. Yan, Y. Sung, P. Krantz, D.K. Kim, J.L. Yoder, T.P. Orlando, S. Gustavsson, and W.D. Oliver. Common framework for optimizing superconducting qubit designs. *In Preparation*, 2020.

[47] Xinyuan You, James A Sauls, and Jens Koch. Circuit quantization in the presence of time-dependent external flux. *Physical Review B*, 99(17):174512, 2019.

[48] B Yurke, LR Corruccini, PG Kaminsky, LW Rupp, AD Smith, AH Silver, RW Simon, and EA Whittaker. Observation of parametric amplification and deamplification in a josephson parametric amplifier. *Physical Review A*, 39(5):2519, 1989.